HHS Public Access

Author manuscript

Spine J. Author manuscript; available in PMC 2024 September 01.

Published in final edited form as:

Spine J. 2023 September ; 23(9): 1375–1388. doi:10.1016/j.spinee.2023.04.012.

Lumbar endplate microfracture injury induces Modic-like changes, intervertebral disc degeneration and spinal cord sensitization – An In Vivo Rat Model

Dalin Wang, MD, PhD[1,2,3,*], **Alon Lai, PhD**[1,*], **Jennifer Gansau, PhD**[1], **Alan C. Seifert, PhD**[4], **Jazz Munitz, BS**[4], **Kashaf Zaheer, BA**[1], **Neharika Bhadouria, MS**[1,5], **Yunsoo Lee, MD**[1], **Philip Nasser, MS**[1], **Damien M. Laudier, BS**[1], **Nilsson Holguin, PhD**[1], **Andrew C. Hecht, MD**[1], **James C. Iatridis, PhD**[1]

[1]Leni and Peter W. May Department of Orthopaedics, Icahn School of Medicine at Mount Sinai, New York, NY

[2]Department of Orthopaedics, Nanjing First Hospital, Nanjing Medical University, Nanjing, Jiangsu, China, 210006

[3]Department of Orthopedic Surgery, University of Kansas Medical Center, 3901 Rainbow Blvd, Kansas City, KS, USA 66160

[4]Biomedical Engineering and Imaging Institute, Department of Radiology, Icahn School of Medicine at Mount Sinai, New York, NY

[5]School of Mechanical Engineering, Purdue University, West Lafayette, IN

Abstract

BACKGROUND CONTEXT: Endplate (EP) injury plays critical roles in painful IVD degeneration since Modic changes (MCs) are highly associated with pain. Models of

Corresponding author: James C. Iatridis, PhD, Leni and Peter W. May Department of Orthopaedics, One Gustave Levy Place, Box 1188, Icahn School of Medicine at Mount Sinai, New York, NY 10029, Tel: +1-212-241-1517, james.iatridis@mssm.edu.

*Authors contributed equally.

Declarations of Competing Interests

The authors declare that they have no known competing financial interests or personal relationships that could have appeared to influence the work reported in this paper.

Supplementary Figure 1: IVD height measured from Faxitron images showing effects of level. L2–3 and L3–4 were uninjured while L4–5 and L5–6 were injured levels. * and **** indicate significant differences with $p<0.05$ and $p<0.0001$ respectively.

Supplementary Figure 2: Hematoxylin and Eosin staining of IVDs showing disruption of IVD structure and inflammatory cell invasion into the IVD in both EP+PBS and EP+TNF injury groups.

Supplemental Figure 3: Surgically-induced EP microfracture resulted marrow changes that were hypointense on T1w and hyperintense on T2w MRI and exhibited secondary damage to the EP. A) Sham, B) EP+PBs, and C) EP+TNFα groups with T1w for 1) sagittal and 2) coronal view and T2w for 3) sagittal and 4) coronal view. EP injuries were apparent on sagittal view on T1w and T2w MRI (blue arrows). EP injuries were also observed as a single lesion location close to middle line on the coronal view (yellow arrow) in both EP injury groups. In the EP+TNFα group, coronal images also showed secondary damage to the cartilage EP regions on coronal (C2) T1w, (C4) T2w in two peripheral lesion locations (white arrow).

EP microfracture that progress to painful conditions are needed to better understand pathophysiological mechanisms and screen therapeutics.

PURPOSE: Establish in vivo rat lumbar EP microfracture model and assess crosstalk between IVD, vertebra and spinal cord.

STUDY DESIGN/SETTING: In vivo rat EP microfracture injury model with characterization of IVD degeneration, vertebral remodeling, spinal cord substance P (SubP), and pain-related behaviors.

METHODS: EP-injury was induced in 5 month-old male Sprague-Dawley rats L4–5 and L5–6 IVDs by puncturing through the cephalad vertebral body and EP into the NP of the IVDs followed by intradiscal injections of TNFα (n=7) or PBS (n=6), compared to Sham (surgery without EP-injury, n=6). The EP-injury model was assessed for IVD height, histological degeneration, pain-like behaviors (hindpaw von Frey and forepaw grip test), lumbar spine MRI and μCT, and spinal cord SubP.

RESULTS: Surgically-induced EP microfracture with PBS and TNFα injection induced IVD degeneration with decreased IVD height and MRI T2 signal, vertebral remodeling, and secondary damage to cartilage EP adjacent to the injury. Both EP injury groups showed MC-like changes around defects with hypointensity on T1-weighted and hyperintensity on T2-weighted MRI, suggestive of MC type 1. EP injuries caused significantly decreased paw withdrawal threshold, reduced axial grip, and increased spinal cord SubP, suggesting axial spinal discomfort and mechanical hypersensitivity and with spinal cord sensitization.

CONCLUSIONS: Surgically-induced EP microfracture can cause crosstalk between IVD, vertebra, and spinal cord with chronic pain-like conditions.

Graphical abstract:

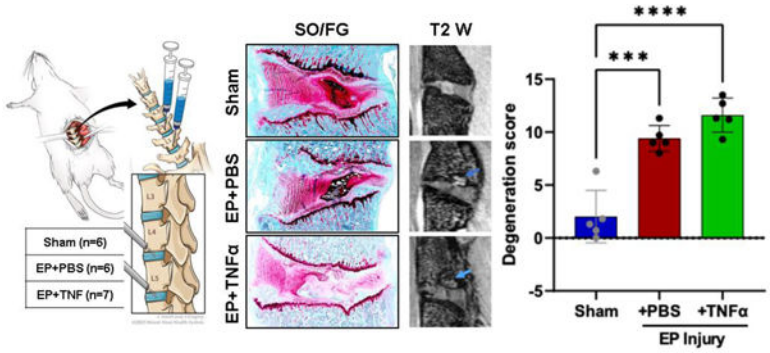

Surgically-induced endplate (EP) microfracture increased IVD degeneration, spinal cord substance P (subP), vertebral remodeling, pain-like behaviors, and resulted in Modic-like EP changes.

Keywords

Intervertebral disc degeneration; Pain; Endplate microfracture; Modic changes; Spinal cord sensitization; In vivo rat model; Spine

Introduction

Chronic back pain is a prevalent musculoskeletal disorder and a major cause of disability with enormous socioeconomic burdens worldwide [1–4]. Back pain is highly associated with endplate (EP) defects in relation to Modic changes (MCs) and intervertebral disc (IVD) degeneration [5–7]. MCs are magnetic resonance imaging (MRI) evidence of inflammatory and fibrotic vertebral bone marrow lesions that associate with adjacent IVD degeneration and EP defects [5, 8–11]. EP defects can involve vertebral body burst fracture or accumulating microfractures at peripheral or central vertebral EP [12]. Many clinical studies identify strong associations between EP defect changes as seen on spinal imaging and pain presence, indicating the importance of these clinically-relevant spinal changes [8, 9, 11, 13]. It is possible that pain from MCs may result from EP microfracture that accumulates into larger EP defects with bone marrow involvement and an autoimmune response due to interactions of IVD with surrounding bone marrow and nervous system tissues [1, 14–20]. A longitudinal investigation of such progressive changes motivates the need for an in vivo model on EP injury.

Animal models are required to identify the causes and to screen potential treatments for pain sources involving EP-driven and annulus fibrosus (AF)-driven IVD degeneration models that are often mixed and interacting in clinical back pain patients [1, 21, 22]. Vertebral EPs and outer annulus fibrosus (AF) are innervated with an abundance of nociceptive neurons that connect to dorsal root ganglion (DRG) and spinal cord. EP defects (or microfracture injury) and elevated pro-inflammatory cytokines from IVD degeneration may irritate nerves in the IVD, vertebrae, or surrounding DRG and spinal cord [23–28]. Clinical MC phenotypes involve pathological changes to IVD and vertebrae, and the relationship of MCs with pain motivates a strong need to develop animal models of EP injury. There are many potential pathophysiological explanations for MC etiology, yet an EP injury model is required to determine if EP microfracture is sufficient to trigger MCs, IVD degeneration and pain [17, 19, 29, 30]. An animal model of EP injury is also needed to identify therapeutic targets that may improve treatments for EP-driven back pain.

Animal models for studying EP injuries have been limited to large animals (i.e. porcine and ovine), with outcome measurements restricted to IVD degeneration, and the effects of EP defects on MCs [31–33]. Large animal models involve a high cost of breeding and housing, and assays to characterize pain-related behaviors are not well-established. Rat models are commonly used to study painful spine conditions because they are relatively inexpensive, have fast healing times, exhibit anatomical and biomechanical similarities to the human spine, and have well-characterized behavioral assays to characterize pain-like conditions [24, 28, 34–42]. Rat models are also sufficiently large to enable spine surgical procedures to be accurately performed. EP defect injuries caused variations in IVD degeneration severity even in large animal models [31–33], suggesting a need for additional models with precisely performed EP injury.

There is a need to determine if an in vivo EP injury model to investigate if EP microfracture is sufficient to cause crosstalk and degenerative remodeling of IVD, vertebrae and spinal cord, and result in pain-like conditions. Therefore, the objectives of this study were to

i) establish and characterize a rat in vivo lumbar EP microfracture injury model, ii) evaluate pain-related behaviors and microstructural characteristics of IVD degeneration and vertebral remodeling from the surgically-induced EP microfracture injury using histology, MRI and μCT, iii) investigate the changes in spinal cord following EP microfracture, and iv) establish associations for EP injury between MRI NP T2 relation time with IVD degeneration, spinal cord SubP and pain-related behaviors. This is the first study to determine if surgically-induced EP microfracture can progress to MCs, IVD degeneration, and spinal cord sensitization with pain-like conditions, and provides an animal model that may be useful to better understand MC-like conditions, their dynamic changes, and potential therapies.

Materials and methods

Study design

All experimental procedures were approved by the Institutional Animal Care and Use Committee. Nineteen 5 month old male Sprague-Dawley rats (Charles River Laboratory, Wilmington, MA) were randomly divided into 3 groups: Sham (n=6), EP+PBS (n=6), EP+TNFα (n=7). EP+PBS and EP+TNFα groups had EP microfracture injury followed by an intradiscal injection of PBS and TNFα, respectively (Figure 1). Surgery was performed for EP injury (n=8 for group) and sham (n=6) with 2 surgical complications on the first EP injury procedures and 1 isoflurane overdose complication at the final sample size that exceeded n=6 required to detect effect sizes as large as our prior AF puncture studies [24]. For the sham group, vertebral bodies between L4-L6 as well as IVD levels L4–5 and L5–6 were exposed without any injury. This study was not designed to distinguish specific roles of IVD and vertebrae in causing these changes but rather to develop an EP microfracture model that resulted in IVD, vertebral, and spinal cord changes with pain-like behaviors. Animals were evaluated for pain-related behaviors throughout the 8 week experimental duration (Figure 2), and were otherwise allowed unrestricted movement in cages. The lumbar spine and spinal cord were then assessed using faxitron for IVD height, histology and IVD degeneration scoring, MRI, μCT, and spinal cord SubP.

Surgical procedure and EP microfracture injury

Surgical procedures were performed under aseptic conditions and general anesthesia via 2% isoflurane (Baxter, Deerfield, IL) [24]. An anterior abdominal incision was used to expose L4~L6 lumbar spine. IVD level was preliminarily identified using preoperative anterior-posterior X-ray images, and confirmed by intraoperative C-arm. Rats underwent either a sham surgical procedure or EP puncture surgery of the L4–5 and L5–6 IVDs. For the EP injury groups, the cephalad EPs of L4–5 and L5–6 IVDs were punctured obliquely from the vertebral body at 1.5 mm cephalad to the edge of IVDs using a 0.6 mm K-wire, which was controlled by a 3 mm depth stopper (Figure 1). All intradiscal injections were performed following the EP injury using a 26-gauge needle with a 3 mm depth stopper. A total of 2.5 ul of PBS or TNFα (0.25 ng in 2.5 ul) (80045RNAE50; Sino Biological Inc., Beijing, China) [24, 43] was then slowly injected into each IVD using a calibrated microliter syringe (Hamilton Company, Reno, NV, USA) following the EP injury. All EP injuries were guided and confirmed radiologically using the C-arm (Figure 1C). Pilot studies refined the

small volumes and slow injection rates to have no detectable resistance. The syringe depth and bevel position were confirmed intraoperatively with the C-arm to be in the center of NP region to enable injectates to be absorbed by the IVD and marrow and minimize the chance of leakage. Using these methods, no leakage was observable visually when injecting blue dye during pilots.

Animals were then housed 2 per cage and maintained at a twelve/twelve hour light/dark cycle (light stage: 7 am to 7 pm) for the experimental duration. Animals were allowed unrestricted movement in cages for the entire experimental duration and co-housed two per cage with the exception of the 24 h post-operative period, when animals were singly housed [28].

von Frey and axial grip behavioral testing

Pain-related behaviors were evaluated using von Frey assay for hindpaw mechanical allodynia at 0, 2, 4, 6 and 8 weeks post-injury, and grip test for axial lumbar discomfort at 0, 1, 3, 5 and 7 weeks post-injury (Figure 2). The behavioral tests were performed by a single experimenter in a dedicated behavioral analysis room with regular indoor lighting.

The mechanical allodynia at hindpaws was assessed using von Frey assay [24, 25, 44];[40]. All rats were acclimated to handling and test cages for 7 consecutive days before testing. On the day of testing, the rats were acclimated in the test cages for 20 min before testing. Von Frey filaments ranging in force between 0.4 and 26.0 g were applied to the plantar surface of each hindpaw in ascending force, with each filament applied five times. The lowest force filament eliciting nocifensive behaviors in 3 out of 5 applications was identified as paw withdrawal threshold. Nocifensive behaviors included paw licking, extended paw withdrawal, and fanning/shaking of the paw. The paw withdrawal thresholds from the left and right hindpaws were averaged for statistical analysis.

Axial lumbar discomfort was assessed using a grip strength test on the forepaws as described by literature [45]. Grip strength was measured using a custom-built testing apparatus with a stainless-steel grid connected to a uniaxial force sensor. During testing, the animal was gently positioned and allowed to grab the metal grid with both forepaws. The tail of the animal was held and gently pulled until the animal released the grid. This action stretches the lumbar spine, and was therefore considered a measure of axial discomfort. The force data was sampled and recorded for 30 seconds using LabVIEW (National Instruments), and the peak force and mean force were calculated via the analysis of the recorded loading curves. This grip force test procedure was repeated three times and each trial was followed by 10 minutes resting with the rats in their own cages. Results were averaged from the three trials at each time point for statistical analysis.

Faxitron analysis of disc height and specimen collection

Changes of IVD height were quantified in vivo using faxitron radiography pre-operatively, and at 8 weeks after injury with the animal anesthetized and carefully placed on its side (Figure 3A) using methods previously described [38]. Care was taken to control for similar anesthesia time and animal placement position between pre-operative and 8 weeks post-surgery time points which showed high repeatability (Supplementary Figure 1). At 8 weeks

post-surgery, all rats were transcardially perfused with 10% buffered formalin phosphate (Fisher Company, Fair Lawn, NJ, USA) under the condition of anesthetization, both lumbar spinal cord and lumbar spines were dissected and fixed in 10% buffered formalin phosphate. The formalin-fixed spinal cord was used for immunohistochemical analysis for substance P; while the fixed spine was for post-mortem MRI and μCT, followed by histological analysis.

MRI scan and analysis

MRI was performed on a 9.4T vertical-bore micro-MRI system (Bruker Avance III 400) using a 20-mm quadrature birdcage RF coil (Rapid Biomedical). T1-weighted (T1w) images were acquired using 3D MP-RAGE (139 μm isotropic resolution, TR=4s, TI=1.1s), T2-weighted (T2w) images were acquired using 3D RARE (139 μm isotropic resolution, TR=2s, TE=17ms), and T2 mapping data were acquired using multi-echo 3D spin-echo (remmiRARE, 250 μm isotropic resolution, TR=520ms, TE1=6ms, ΔTE=5ms, 32 echoes). T1w and T2w images were analyzed for Modic changes using methods previously described [10, 46].

T2 maps were produced by fitting a single exponential decay to each voxel's echo train. Using co-registered anatomical images as a guide, 3D regions of interest (ROI) in the NP, whole IVD, and bone marrow were defined on T2 maps as binary masks using FSLEyes (https://fsl.fmrib.ox.ac.uk/fsl/fslwiki/FSLeyes). Mean values for T2 relaxation time were quantified within each mask, excluding voxels where quality of fit was poor due to insufficient signal (e.g., bone), using fslstats, a utility contained within FSL [47, 48]. The 3D ROIs for NP and whole IVD T2map masks were manually drawn in FSLEyes to enclose the entire NP and IVD using T2w and T1w co-registered images that easily identified the borders of these anatomic structures. The 3D ROI for the bone marrow was created using a 5-voxel cube centered on the endplate defect region, which was then manually cropped to exclude non-marrow tissues (e.g., IVD and cortical bone). Since the Large ROI 5-voxel cube averaged regions beyond the localized injury, we also created a Small ROI using a 3-voxel cube centered on the brightest area of the EP defect, and on comparable region in the sham animals (which did not exhibit defects). These smaller ROIs did not require cropping to exclude non-marrow tissues. All ROIs were identified by researchers who were blinded to the experimental group.

μCT scan and analysis

Vertebral body remodeling was assessed via μCT at 8 weeks post-surgery. μCT was performed on a Nanoscan PET/CT system (Mediso Co) at energy 84 uAs, slice thickness of 0.02 mm, isotropic voxel size at 0.25 mm. Image analysis was performed using Osirix MD, version 11.0. After opening reconstructed CT images, scans were viewed in a sagittal orientation, and 3 volumetric ROIs were hand drawn in each vertebra. The injury site ROIs characterized the endplate regions, and were drawn using the pencil tool extending from the inner corona of the injury area extending 1 mm along the endplate, and extended horizontally alongside the trabecular area of the bone. For Adjacent ROI regions, sections were drawn beginning 1 mm above the injury site, and extended 1 mm in height, and horizontally along the width of the trabecular region. The Far Field ROIs were drawn mirroring the size and position of the endplate region, on the endplate on the opposite

side of the vertebral body. The 3D ROIs were modeled, and the volume was noted. A histogram of pixel-binned values was created, and all values above 1000 Hounsfield counts (experimentally determined to represent trabecular bone) were counted as bone volume (BV) voxels, and this was compared to the total voxel counts within the ROI, or total volume (TV). BV/TV was calculated, and presented in comparison between the three regions selected for analysis. ROIs were created and analyses performed by researchers who were blinded for the experimental group.

Histology, IVD degeneration score, and immunohistochemical analyses of spinal cord

After the MRI and μCT scanning, the fixed specimens were decalcified, embedded in resin, and sectioned sagittally at 5 μm intervals. The midsagittal section with the EP microfracture were identified, and stained with Safranin-O/fastgreen/hematoxylin for disc morphology and glycosaminoglycan (GAG) content; and with hematoxylin and eosin for IVD cellularity. Slides were then imaged using bright-field microscopy (Leica Microsystems, Inc, Deerfield, IL, USA). IVD degeneration score was determined using a grading system that evaluated NP morphology, NP cellularity, NP-AF border, AF morphology, and EP irregularity [49]. IVD degeneration scoring was performed with three evaluators, who were blinded to the experimental groups, and the degeneration score from the three evaluators were averaged for statistical analysis.

The formalin-fixed spinal cords were paraffin-embedded and sectioned sagittally at 5 μm intervals. Two sections per animal spread across the lumbar spinal cord were selected. After deparaffinization and rehydration, the spinal cord sections were treated with antigen-retrieval buffer, Histo/zyme (H3292, Sigma-Aldrich, Inc, St. Louis, MO, USA), and protein blocking buffer, 2.5% normal horse serum (S-2012, Vector Laboratories, Inc, Burlingame, CA, USA). Sections were incubated at room temperature for one hour with mouse monoclonal primary antibodies against rat substance P (1:300 dilution, ab14184, Abcam, Cambridge, MA, USA) or normal mouse serum (ab7486, Abcam) as negative control [24]. After incubation with RTU biotinylated goat anti-mouse IgG secondary antibody (BP-9200, Vector Laboratories, Inc), the sections were treated with DyLight 488 horse anti-goat IgG antibody (DI-3088, Vector Laboratories, Inc). The sections were then Nissl-stained to visualize the neurons and glia cells, washed and mounted (ProLong™ Gold Antifade Mountant with DAPI, P36931, Thermo Fisher Scientific, Waltham, MA, USA). Images were taken at 20x magnification using Leica DM6 B microscope (Leica Microsystems, Inc). Identical microscope settings were used throughout. All images were analyzed using ImageJ, an immunoreactivity (ir) threshold was set and the percentage of SubP-ir relative to area of spinal dorsal horn was quantified, and then averaged between left and right dorsal horn as well as across the two sections from each animal.

Statistical analyses

All post-injury data of IVD heights, paw withdrawal thresholds and grip strengths were normalized to pre-injury values and presented as percent change to minimize individual variability. Normalized IVD height, spine MRI, μCT, IVD degeneration score, and spinal cord immunohistochemistry were analyzed using one-way ANOVA with Tukey's multiple comparison test. Pearson's correlation analyses identified associations between

IVD height, T2 signal, BV/TV, IVD degeneration grade, spinal cord SubP, hindpaw withdrawal threshold, and grip peak force in order to determine the crosstalk across different tissues following EP injury as well as their contributions to the changes in pain-related behaviors. All statistical analyses were performed using Prism (GraphPad, LaJolla, CA), with significance level set as $\alpha = 0.05$.

Results

Surgery did not affect rat general health

Both sham surgery and EP injury procedures were well-tolerated by the rats. The rat body weight averaged 561±34g, 568±33g, 579±29g, 592±33g, and 611±35g, for pre-surgery and post-surgery weeks 2, 4, 6, and 8, respectively. There were no significant differences between groups at each time point. No obvious stress or discomfort were observed from the general physical examination.

EP microfracture induced back pain-related behavior

Both groups involving EP injury with either PBS or TNFα had significantly decreased paw withdrawal threshold at hindpaw compared to Sham (Figure 2A), demonstrating increased mechanical sensitivity at the hindpaw and suggesting central sensitization. Both injured groups had significantly decreased forelimb peak grip force and mean grip force compared to Sham at all postoperative timepoints (Figure 2B and C), demonstrating increased axial discomfort. Sham rats did not show significant changes in pain-related behaviors with time. Results of the von Frey and axial grip test together suggest increased pain sensitivity after both EP injury types.

EP microfracture induced IVD degeneration

At 8 weeks post-surgery, changes in IVD height were significantly different among the three groups: At L4–5, EP+TNFα group decreased to 86.3%±4.9% of baseline, EP+PBS group decreased to 92.8%±3.4%, while the Sham group increased slightly to 100.4%±2.4%. At L5–6, EP+TNFα group decreased to 76.5%±11.5% of baseline, EP+PBS group decreased to 92.5%±3.1%, while the Sham group decreased slightly to 96.7%±2.7%. There was no apparent change in IVD height in the Sham group or at internal control levels (ie, L2–3 and L3–4) that were not injured (Supplementary Figure 1).

Normal IVD morphology was observed in sham surgery animals, while EP injuries with intradiscal injections of PBS or TNFα induced moderate to severe IVD degenerative changes, including smaller and more fibrous NP, decreased number of NP cells, less distinct NP-AF boundaries, disorganized AF lamellae, and observable EP disruptions (Figure 4A). The EP injury groups exhibited degenerated NP and/or fibrotic tissue that herniated into the adjacent vertebra through the damaged EP, as well as fibrotic remodeling around the damaged EP as well as fibrotic remodeling around the EP injury region (Figure 4A, Supplementary Figure 2). There were minimal to no AF tears or disruptions as the AF was kept intact during IVD injury. The semi-quantitative degeneration grading system showed that Sham IVDs had low Total IVD degeneration scores (2.0±2.5, Figure 4B). IVD degeneration scores of both EP+PBS (9.4±1.2) and EP+TNFα (11.6±1.6) injury groups

were significantly higher than that of the Sham group ($p<0.05$). The scores of subcategories of NP morphology, NP cellularity, NP-AF border and EP of the EP injury groups were significantly higher than the Sham group.

MRI measures of IVD degeneration were performed with mean T2 relaxation time, calculated from T2maps. NP T2 relaxation times tissue significantly decreased with EP+TNFα compared to Sham and EP+PBS, respectively (Figure 5). T2 values of the whole IVD were not affected by the injury, highlighting the localized nature of this injury (Figure 5).

EP microfracture induced Modic-like changes and bone remodeling

Post-mortem MRI at 8 weeks showed IVD degeneration and bone marrow signal changes. EP defects were observed that had characteristics similar to Modic-like changes and reactive Schmorl's nodes defects. Modic-like changes were visible in both EP injury groups with obvious qualitative appearance on MRI exhibiting hypointensity on T1w images and hyperintensity on T2w images (Figure 5A), suggestive of MC type 1. T2 mapping sequences also indicated reduced T2 signal in the NP region of the EP+TNFα group but not for the whole IVD indicating reduced NP water content and greatest severity of IVDD (Figure 5B and C). However, T2 mapping showed no differences in T2 relaxation times for the large ROI across groups while the small ROI focused on the EP microfracture region detected a significantly increased EP T2 signal for the EP+PBS group. The increased EP T2 signal indicated increased water in the vicinity of the EP microfracture which could suggest more inflammation or NP herniation through the EP defect into the adjacent vertebra. The EP+TNFα group also showed Modic-like changes, although T1w and T2w images demonstrated larger and more diffuse changes suggesting EP remodeling and inflammation with involvement of IVD and vertebral compartments (Supplementary Figure 3). A larger and more diffuse inflammatory pattern can also explain the slightly lower T2 signal in EP+TNFα compared to EP+PBS in the EP small ROI.

The μCT analyses showed trabecular bone remodeling in both EP injury groups (Figure 6A and B), and cartilage EP secondary damage in the EP+TNFα group that was most obvious on histological images (Figure 4A). Mean values of BV/TV (%) decreased after EP injury compared to Sham at the injury site, adjacent site, and far field in the vertebrae regions (Figure 6C), although these decreases were significantly different in the far field ($p<0.05$) and statistical trends ($p<0.1$) in the injury and adjacent sites (likely due to the limited sample size on this analysis).

EP microfracture increased SubP in spinal dorsal horn

SubP, a pain-related neurotransmitter produced from nociceptive neurons, was mainly localized in laminae I and II of the spinal cord dorsal horn (Figure 7A). The percentage area of SubP-ir (relative to dorsal horn) was significantly increased in rat spinal dorsal horns from EP injury groups (3.61%±0.82% and 3.88%±0.69% for EP+PBS and EP+TNF groups, respectively) compared to that of Sham (2.15%±0.65%) (Figure 7C).

EP microfracture caused crosstalk between IVD, vertebra and spinal cord and degenerative changes to all 3 tissues associated with pain-like behaviors

Surgically-induced EP microfracture resulted in MRI NP T2 signal that significantly correlated with μCT BV/TV at injured EP suggesting EP injury interacts with NP water content (Table 1). NP T2 relaxation times also significantly correlated with histological IVD degeneration and spinal cord SubP indicating cross-talk between IVD and spinal cord due to this EP microfracture injury (Figure 8). NP T2 also correlated with hindpaw von Frey and axial grip force, indicating an association of NP T2 times with pain-like behaviors. The IVD degeneration score also significantly correlated with μCT BV/TV at the site adjacent to the injury, suggesting IVD and vertebrae may both remodel following surgically-induced EP injury. Spinal cord SubP significantly correlated with NP T2 signal, IVD height, and μCT BV/TV at the EP site, suggesting associations between the degenerative changes of spinal cord, IVD and EP. The multiple associations between IVD, vertebra, and spinal cord suggest crosstalk between all of these tissues (Table 1).

Pain-related behaviors significantly correlated with degenerative changes in IVD, vertebrae and spinal cord (Table 2). Specifically, the hindpaw withdrawal threshold significantly correlated with MRI NP T2, IVD degeneration score, and spinal cord SubP while the axial grip force significantly correlated with relative IVD height, IVD degeneration score, μCT BV/TV at adjacent site, and spinal cord SubP.

Discussion

Current clinical diagnoses for EP-driven IVD degeneration lacks phenotypic precision, has a high incidence of pain, and treatments have limited efficacy [50, 51]. A rat in vivo EP-driven IVD degeneration model was developed to better understand the progression of EP defects to EP-driven IVD degeneration, chronic pain and cross-talk between spinal tissues. We created a transcorporeal EP injury with a size of ~2% of the average rat lumbar EP surface area [52], which we describe as a microfracture injury. This is the first in vivo study to apply a surgically-induced EP microfracture injury, and we show this can cause degenerative remodeling of IVD, vertebrae and spinal cord. This is also a first study to investigate pain from such conditions and we show that pain-related behaviors significantly correlated with measures of IVD degeneration, EP changes, and spinal cord SubP, suggesting EP microfracture injury can cause pain-like conditions with crosstalk between vertebrae, IVD and spinal cord. The EP lesion was characterized to be hyperintense on T2w and hypointense on T1w, and histology showed fibrotic remodeling and inflammatory cell infiltration, suggesting similarities to MC type 1 conditions. The chronic and persistent pain-related behavior phenotype with hindpaw sensitivity and increased spinal cord SubP further suggested central sensitization. This EP microfracture injury induces changes to IVD, vertebra and spinal cord that all warrant some consideration during diagnosis and treatment for conditions with EP defects.

This EP injury model was characterized using imaging modalities and defined MC presence and severity using MRI [46] that provides parallels to the human clinical condition. MCs are vertebral endplate and adjacent bone marrow lesions visible via MRI, and their three phenotypes (MCs type1, MCs type2, MCs type3) were first described by de Roos et

al. [53] and Modic et al. [10]. MC type 1 (hyperintense on T2w, hypointense on T1w) reflect inflammatory and fibrotic lesions and have the highest association with pain; MC type 2 (hyperintense on T1w and T2w) are associated with fatty replacement of the bone marrow; while MC type 3 (hypointense on T1w and T2w,) involve marrow sclerosis and are often asymptomatic [29]. EP injury is described to occur through traumatic fractures or accumulating microfractures with MCs. MCs prevalence is high in patients with back pain and EP injury [54–56]. Schmorl's nodes can be defined as a localized vertebral EP irregularity, commonly including herniation of NP through the EP into the vertebra, although their origin and relevance to painful pathologies are less clear [57, 58]. Nevertheless, considerable variation exists in nomenclature, etiology, and degree of severity of the EP defects [59]. Clinically, MC type 1 may reflect a state of active degeneration with back pain that could be related to biomechanical instability, inflammation, or other causes that are often considered poorly indicated for surgical intervention [17, 29, 46, 60–62].

In the current study, EP microfracture caused MC-like changes to the vertebra involving hypointensity on T1w and hyperintensity on T2w as well as qualitative marrow edema on the T2 map (Figure 5), which all suggest MC-like changes most similar to MC type 1. However, the EP T2 relaxation times were only significantly increased locally in the small ROI, suggesting either localized inflammation and/or herniation of degenerated NP tissue into the vertebral space (Figure 4) which could also suggest a reactive Schmorl's node and/or combined phenotype. The MC-like changes were more easily visible when comparing EP+TNFα with Sham on T2w and T1w images than with EP+PBS group which were predominantly visible on T2w MRI. Nevertheless, EP changes were apparent on MRI in all injured samples, and histology further demonstrated MC-like changes with accumulation of fibrotic tissue and inflammatory cell accumulation that was more severe for EP+TNFα than EP+PBS (Figure 4; Supplementary Figure 2), and was suggestive of MC type 1. The enhanced degenerative remodeling from TNFα injection further suggests MC type 1-like changes since Dudli et al. showed that proinflammatory stimulus was critical to induce MC1-like changes [29]. Another EP injury study, just published, showed CD68+ macrophages were significantly increased in the vertebral body and EP injury region, further indicating inflammation cell involvement [63]. Future studies that more precisely characterize immune cells and fibrotic proteins around the EP microfracture would enable closer comparison with the human condition, for example by measuring CD90+ stromal cells which were identified in the inflammatory and fibrotic changes in human MCs type 1 [64]. MC types can be dynamic and inter-convertible, and in this study we therefore believe the characterization of MC-type and/or reactive Schmorl's node is less important than the evidence that this EP microfracture results in alterations in IVD, vertebra and spinal cord with a pain-like phenotype., and This study also builds on the MC literature that shows EP fractures can cause inflammatory and catabolic changes, which are suggested to occur from an autoimmune response of the bone marrow against the IVD [18, 29, 31, 54, 55]. [64]

The pain-related behavioral phenotype was characterized with reduced axial grip strength and increased mechanical sensitivity at the hindpaw suggesting local and central pain [65]. PBS and TNFα injections had identical behavioral results, indicating that the behavioral phenotypes were affected by the presence of the EP puncture injury, and not the type of injectate. Results therefore suggest that the EP puncture injury itself causes pain or disability

that may be a result of EP-injury induced axial instability or inflammation. The grip force assay requires contraction of axial musculature for the animal to stabilize and grip the bar. The significant reduction in grip force is most likely related to axial mechanical discomfort and/or disability since previous EP injury showed axial biomechanical instability in rat spinal segments in ex vivo biomechanical tests [66]. NP contact through the EP injury into the highly innervated vertebral tissue is another potential source of such axial discomfort since the hydrophilic NP can swell into this space and/or induce an inflammatory response. Results therefore suggest MC-like changes, as induced in this model, may have an axial pain phenotype with mechanical and inflammatory contributions.

Central sensitization was suggested by increased spinal cord SubP as well as decreased mechanical withdrawal threshold at the hindpaw (i.e., mechanical hypersensitivity that is not at the injury site), since there was no evidence that this vertebral EP puncture injury resulted in spinal cord or nerve root compression from herniation or vertebral remodeling on imaging or histology. However, inflammatory conditions were observed with EP injury, with the presence of inflammatory cells, and MC1-like changes with increased spinal cord SubP-ir 8 weeks after EP microfracture injury. The SubP in the spinal cord were mainly at laminae I and II which include terminations of nociceptive A-delta and C nerve fibers [67]. Spinal cord SubP is increased from direct spinal cord injury [68] or spinal transection [69], from diabetic neuropathy models [70], and also following paw inflammatory injury [71], suggesting spinal cord sensitization can occur from inflammatory and neuropathic sources in the spinal cord or periphery. The current study adds EP microfracture injury to the list of conditions that may result in spinal cord sensitization.

EP+PBS and EP+TNFα groups had similar pain-like behavioral responses even though EP+TNFα had more severe Modic-like changes and IVD degeneration score. Results therefore suggest that pain and disability may be driven more by the presence of the EP injury rather than the injection type, although it remains likely that the more severe EP+TNFα condition would reduce healing potential and perhaps cause greater dysfunction at longer time points in this model. In context of the literature, EP microfracture injury causes inflammatory and marrow changes and central spinal cord sensitization. The pain-related behavior in our model is therefore most likely related to biomechanical instability as well as inflammation, suggesting important parallels with the human clinical condition.

Imaging results allow us to confirm that the EP defect was a local microfracture injury that resulted in a broader inflammatory response. However, quantitative analyses of vertebral BV/TV or marrow T2 relaxation times did not detect statistical differences due to the limited sample size, particularly for μCT which occurred on a subset of the samples (3 sham; 3 EP+PBS and 5 EP+TNFα) because of a technical error when a batch of samples were mistakenly embedded for histology prior to scanning. Trabecular microstructure remodeling occurred following surgically-induced EP microfracture as apparent on imaging, and there was a suggestion that trabecular remodeling occurred throughout the entire affected vertebra, even though quantitative results were inconclusive. This study therefore has similarities to the human condition, as Senck et al., used μCT to visualize EP-driven IVD degeneration and demonstrated a local increase of trabecular thickness inferior to the EP collapse, and trabecular microstructure in the immediate vicinity of the collapse seems to be less

organized, showing thicker trabeculae with a decreased trabecular length [22]. It is expected that BV/TV would be decreased in both EP injury groups due to bone absorption and remodeling caused by bone marrow/NP autoimmunity reaction.

Some limitations are important to highlight. The human clinical condition accumulates over decades, while all surgically induced animal models involve acute injuries. This EP microfracture injury study was designed to have some similarities with the human MC clinical condition, including sustained pain-like behaviors with multi-compartment degeneration of the spine with chronic changes to IVD, vertebrae and the spinal cord. EP microfracture was induced using a transcorporeal approach by one experienced spine surgeon and fluoroscopy guidance to enhance precision with injection. The EP microfracture injury model therefore induces changes that could be related to EP microfracture, transcorporeal vertebral injury, and/or IVD injection. This study was not designed to distinguish specific roles of IVD and vertebrae in causing these changes, yet an experimental group with vertebral injury that does not penetrate the EP would be an interesting control to allow such distinction in future studies. Furthermore, the transcorporeal approach disrupted the vertebra/marrow, so that we can only conclude that the vertebral changes are due to the entire EP microfracture injury procedure and not EP microfracture alone. Lastly, the ventral approach to create a central EP injury has some differences from the human degenerative conditions that can involve dorsal vertebrae, IVD and/or EP changes. It is notable that the effects of this EP microfracture injury in this model are more severe than prior studies that investigated AF puncture injury with similar PBS and TNFα injection [24]. We cannot exclude the possibility that injectate leakage caused some of the observed effects, but believe effects of injectate leakage would be a very small contributor to the chronic changes presented since several pilot studies refined this surgical method and injection procedure so that no acute leakage of injectate with dye was visible. The injection had no resistance pressure during surgery, although it is possible that acute swelling from the procedure resulted in some of the pain-like behaviors and pathology observed in this model. In this context, we started to assess the pain-like behavior at 7d or 14d post-surgery after any swelling would have subsided instead of immediately post-op stage. This study used male rats because of their larger size that made surgery slightly easier, and their more well-characterized von Frey mechanical sensitivity to IVD disruptions [24, 65]. Future studies are required to include female rats to improve the generalizability of these findings. Lastly, this is a descriptive model characterization study, and we hope this model will be able to gain further insights into discogenic pain with future blocking and therapeutic screening studies.

Conclusions

This study established a rat in vivo model where surgically-induced EP microfracture caused IVD degeneration, vertebral remodeling, and spinal cord sensitization. Surgically-induced EP microfracture resulted in crosstalk between vertebrae, IVD, and spinal cord since changes to all three structures correlated with each other. The pain-like behaviors also correlated with changes to IVD, vertebra and spinal cord measurements, and were dependent on the presence of EP injury and not injection type. The behavioral, radiological and histological phenotypes of this model had several similarities with MC-like changes in the

human clinical condition, suggesting EP defects can cause painful conditions related to the crosstalk and degeneration of IVD vertebral, and spinal cord structures.

Supplementary Material

Refer to Web version on PubMed Central for supplementary material.

Acknowledgement

This work was funded by grants from the National Institute of Arthritis and Musculoskeletal and Skin Diseases NIH/NIAMS grants R01AR078857 (~$600k to the institution) & R01AR080096 (~$600k to the institution) (JCI, ACH, AL). Development of the remmiRARE pulse sequence was funded by NIH/NIBIB grant R01EB019980 (~$500k) (AS). AH received royalties of $5k unrelated to the content of this project. No other funding sources contributed to this project, and therefore no other potential sources of bias are present for this study.

References

1. Adams MA, Dolan P. Intervertebral disc degeneration: evidence for two distinct phenotypes. J Anat 2012;221(6):497–506. [PubMed: 22881295]
2. Battie MC, Videman T, Levalahti E, Gill K, Kaprio J. Genetic and environmental effects on disc degeneration by phenotype and spinal level: a multivariate twin study. Spine (Phila Pa 1976) 2008;33(25):2801–8. [PubMed: 19050586]
3. Hoy D, March L, Brooks P, et al. The global burden of low back pain: estimates from the Global Burden of Disease 2010 study. Ann Rheum Dis 2014;73(6):968–74. [PubMed: 24665116]
4. Wang D, Yuan H, Liu A, et al. Analysis of the relationship between the facet fluid sign and lumbar spine motion of degenerative spondylolytic segment using Kinematic MRI. Eur J Radiol 2017;94:6–12. [PubMed: 28941762]
5. Zehra U, Cheung JPY, Bow C, Lu W, Samartzis D. Multidimensional vertebral endplate defects are associated with disc degeneration, modic changes, facet joint abnormalities, and pain. J Orthop Res 2019;37(5):1080–9. [PubMed: 30515862]
6. Mallow GM, Zepeda D, Kuzel TG, et al. ISSLS PRIZE in Clinical Science 2022: Epidemiology, risk factors and clinical impact of juvenile Modic changes in paediatric patients with low back pain. Eur Spine J 2022;31(5):1069–79. [PubMed: 35129673]
7. Jensen TS, Karppinen J, Sorensen JS, Niinimaki J, Leboeuf-Yde C. Vertebral endplate signal changes (Modic change): a systematic literature review of prevalence and association with non-specific low back pain. Eur Spine J 2008;17(11):1407–22. [PubMed: 18787845]
8. Braten LCH, Rolfsen MP, Espeland A, et al. Efficacy of antibiotic treatment in patients with chronic low back pain and Modic changes (the AIM study): double blind, randomised, placebo controlled, multicentre trial. BMJ 2019;367:l5654. [PubMed: 31619437]
9. Herlin C, Kjaer P, Espeland A, et al. Modic changes-Their associations with low back pain and activity limitation: A systematic literature review and meta-analysis. PLoS One 2018;13(8):e0200677. [PubMed: 30067777]
10. Modic MT, Steinberg PM, Ross JS, Masaryk TJ, Carter JR. Degenerative disk disease: assessment of changes in vertebral body marrow with MR imaging. Radiology 1988;166(1 Pt 1):193–9. [PubMed: 3336678]
11. Yang X, Karis DSA, Vleggeert-Lankamp CLA. Association between Modic changes, disc degeneration, and neck pain in the cervical spine: a systematic review of literature. Spine J 2020;20(5):754–64. [PubMed: 31731008]
12. Lotz JC, Fields AJ, Liebenberg EC. The role of the vertebral end plate in low back pain. Global Spine J 2013;3(3):153–64. [PubMed: 24436866]
13. Maatta JH, Wadge S, MacGregor A, Karppinen J, Williams FM. ISSLS Prize Winner: Vertebral Endplate (Modic) Change is an Independent Risk Factor for Episodes of Severe and Disabling Low Back Pain. Spine (Phila Pa 1976) 2015;40(15):1187–93. [PubMed: 25893353]

14. Albert HB, Kjaer P, Jensen TS, Sorensen JS, Bendix T, Manniche C. Modic changes, possible causes and relation to low back pain. Med Hypotheses 2008;70(2):361–8. [PubMed: 17624684]
15. Crock HV. Internal disc disruption. A challenge to disc prolapse fifty years on. Spine (Phila Pa 1976) 1986;11(6):650–3. [PubMed: 3787337]
16. Dudli S, Boffa DB, Ferguson SJ, Haschtmann D. Leukocytes Enhance Inflammatory and Catabolic Degenerative Changes in the Intervertebral Disc After Endplate Fracture In Vitro Without Infiltrating the Disc. Spine (Phila Pa 1976) 2015;40(23):1799–806. [PubMed: 26571062]
17. Dudli S, Fields AJ, Samartzis D, Karppinen J, Lotz JC. Pathobiology of Modic changes. Eur Spine J 2016;25(11):3723–34. [PubMed: 26914098]
18. Dudli S, Sing DC, Hu SS, et al. ISSLS PRIZE IN BASIC SCIENCE 2017: Intervertebral disc/bone marrow cross-talk with Modic changes. Eur Spine J 2017;26(5):1362–73. [PubMed: 28138783]
19. Kerttula LI, Serlo WS, Tervonen OA, Paakko EL, Vanharanta HV. Post-traumatic findings of the spine after earlier vertebral fracture in young patients: clinical and MRI study. Spine (Phila Pa 1976) 2000;25(9):1104–8. [PubMed: 10788855]
20. Rajasekaran S, Babu JN, Arun R, Armstrong BR, Shetty AP, Murugan S. ISSLS prize winner: A study of diffusion in human lumbar discs: a serial magnetic resonance imaging study documenting the influence of the endplate on diffusion in normal and degenerate discs. Spine (Phila Pa 1976) 2004;29(23):2654–67. [PubMed: 15564914]
21. Adams MA, Roughley PJ. What is intervertebral disc degeneration, and what causes it? Spine 2006;31(18):2151–61. [PubMed: 16915105]
22. Senck S, Trieb K, Kastner J, Hofstaetter SG, Lugmayr H, Windisch G. Visualization of intervertebral disc degeneration in a cadaveric human lumbar spine using microcomputed tomography. J Anat 2020;236(2):243–51. [PubMed: 31670389]
23. Krock E, Millecamps M, Currie JB, Stone LS, Haglund L. Low back pain and disc degeneration are decreased following chronic toll-like receptor 4 inhibition in a mouse model. Osteoarthritis Cartilage 2018;26(9):1236–46. [PubMed: 29908959]
24. Lai A, Moon A, Purmessur D, et al. Annular puncture with tumor necrosis factor-alpha injection enhances painful behavior with disc degeneration in vivo. Spine J 2016;16(3):420–31. [PubMed: 26610672]
25. Lai A, Ho L, Evashwick-Rogler TW, et al. Dietary polyphenols as a safe and novel intervention for modulating pain associated with intervertebral disc degeneration in an in-vivo rat model. PLoS One 2019;14(10):e0223435. [PubMed: 31577822]
26. Leimer EM, Gayoso MG, Jing L, Tang SY, Gupta MC, Setton LA. Behavioral Compensations and Neuronal Remodeling in a Rodent Model of Chronic Intervertebral Disc Degeneration. Sci Rep 2019;9(1):3759. [PubMed: 30842475]
27. Miyagi M, Ishikawa T, Orita S, et al. Disk injury in rats produces persistent increases in pain-related neuropeptides in dorsal root ganglia and spinal cord glia but only transient increases in inflammatory mediators: pathomechanism of chronic diskogenic low back pain. Spine (Phila Pa 1976) 2011;36(26):2260–6. [PubMed: 21228748]
28. Mosley GE, Wang M, Nasser P, et al. Males and females exhibit distinct relationships between intervertebral disc degeneration and pain in a rat model. Sci Rep 2020;10(1):15120. [PubMed: 32934258]
29. Dudli S, Liebenberg E, Magnitsky S, Lu B, Lauricella M, Lotz JC. Modic type 1 change is an autoimmune response that requires a proinflammatory milieu provided by the ‘Modic disc’. Spine J 2018;18(5):831–44. [PubMed: 29253635]
30. Han C, Wang T, Jiang HQ, et al. An Animal Model of Modic Changes by Embedding Autogenous Nucleus Pulposus inside Subchondral Bone of Lumbar Vertebrae. Sci Rep 2016;6:35102. [PubMed: 27713567]
31. Cinotti G, Della Rocca C, Romeo S, Vittur F, Toffanin R, Trasimeni G. Degenerative changes of porcine intervertebral disc induced by vertebral endplate injuries. Spine (Phila Pa 1976) 2005;30(2):174–80. [PubMed: 15644752]
32. Holm S, Holm AK, Ekstrom L, Karladani A, Hansson T. Experimental disc degeneration due to endplate injury. J Spinal Disord Tech 2004;17(1):64–71. [PubMed: 14734978]

33. Vadala G, Russo F, De Strobel F, et al. Novel stepwise model of intervertebral disc degeneration with intact annulus fibrosus to test regeneration strategies. J Orthop Res 2018;36(9):2460–8. [PubMed: 29603340]
34. Elliott DM, Sarver JJ. Young investigator award winner: validation of the mouse and rat disc as mechanical models of the human lumbar disc. Spine (Phila Pa 1976) 2004;29(7):713–22. [PubMed: 15087791]
35. Hwang PY, Allen KD, Shamji MF, et al. Changes in midbrain pain receptor expression, gait and behavioral sensitivity in a rat model of radiculopathy. Open Orthop J 2012;6:383–91. [PubMed: 22962568]
36. Kim JS, Kroin JS, Buvanendran A, et al. Characterization of a new animal model for evaluation and treatment of back pain due to lumbar facet joint osteoarthritis. Arthritis Rheum 2011;63(10):2966–73. [PubMed: 21953085]
37. Kim JS, Kroin JS, Li X, et al. The rat intervertebral disk degeneration pain model: relationships between biological and structural alterations and pain. Arthritis Res Ther 2011;13(5):R165. [PubMed: 21996269]
38. Lai A, Moon A, Purmessur D, et al. Assessment of functional and behavioral changes sensitive to painful disc degeneration. J Orthop Res 2015;33(5):755–64. [PubMed: 25731955]
39. Miyagi M, Ishikawa T, Kamoda H, et al. Assessment of pain behavior in a rat model of intervertebral disc injury using the CatWalk gait analysis system. Spine (Phila Pa 1976) 2013;38(17):1459–65. [PubMed: 23649215]
40. Mosley GE, Hoy RC, Nasser P, et al. Sex Differences in Rat Intervertebral Disc Structure and Function Following Annular Puncture Injury. Spine (Phila Pa 1976) 2019.
41. Rousseau MA, Ulrich JA, Bass EC, Rodriguez AG, Liu JJ, Lotz JC. Stab incision for inducing intervertebral disc degeneration in the rat. Spine 2007;32(1):17–24. [PubMed: 17202887]
42. Zhang KB, Zheng ZM, Liu H, Liu XG. The effects of punctured nucleus pulposus on lumbar radicular pain in rats: a behavioral and immunohistochemical study. J Neurosurg Spine 2009;11(4):492–500. [PubMed: 19929348]
43. Ponnappan RK, Markova DZ, Antonio PJ, et al. An organ culture system to model early degenerative changes of the intervertebral disc. Arthritis Res Ther 2011;13(5):R171. [PubMed: 22018279]
44. Evashwick-Rogler TW, Lai A, Watanabe H, et al. Inhibiting tumor necrosis factor-alpha at time of induced intervertebral disc injury limits long-term pain and degeneration in a rat model. JOR Spine 2018;1(2).
45. Miyagi M, Millecamps M, Danco AT, Ohtori S, Takahashi K, Stone LS. ISSLS Prize winner: Increased innervation and sensory nervous system plasticity in a mouse model of low back pain due to intervertebral disc degeneration. Spine (Phila Pa 1976) 2014;39(17):1345–54. [PubMed: 24718079]
46. Udby PM, Samartzis D, Carreon LY, Andersen MO, Karppinen J, Modic M. A definition and clinical grading of Modic changes. J Orthop Res 2022;40(2):301–7. [PubMed: 34910328]
47. Smith SM, Jenkinson M, Woolrich MW, et al. Advances in functional and structural MR image analysis and implementation as FSL. Neuroimage 2004;23 Suppl 1:S208–19. [PubMed: 15501092]
48. Jenkinson M, Beckmann CF, Behrens TE, Woolrich MW, Smith SM. Fsl. Neuroimage 2012;62(2):782–90. [PubMed: 21979382]
49. Lai A, Gansau J, Gullbrand SE, et al. Development of a standardized histopathology scoring system for intervertebral disc degeneration in rat models: An initiative of the ORS spine section. JOR Spine 2021;4(2):e1150. [PubMed: 34337335]
50. Hao L, Li S, Liu J, Shan Z, Fan S, Zhao F. Recurrent disc herniation following percutaneous endoscopic lumbar discectomy preferentially occurs when Modic changes are present. J Orthop Surg Res 2020;15(1):176. [PubMed: 32410638]
51. Lurie JD, Moses RA, Tosteson AN, et al. Magnetic resonance imaging predictors of surgical outcome in patients with lumbar intervertebral disc herniation. Spine (Phila Pa 1976) 2013;38(14):1216–25. [PubMed: 23429684]

52. Jaumard NV, Leung J, Gokhale AJ, Guarino BB, Welch WC, Winkelstein BA. Relevant Anatomic and Morphological Measurements of the Rat Spine: Considerations for Rodent Models of Human Spine Trauma. Spine (Phila Pa 1976) 2015;40(20):E1084–92. [PubMed: 26731709]

53. de Roos A, Kressel H, Spritzer C, Dalinka M. MR imaging of marrow changes adjacent to end plates in degenerative lumbar disk disease. AJR Am J Roentgenol 1987;149(3):531–4. [PubMed: 3497539]

54. Adams MA, Freeman BJ, Morrison HP, Nelson IW, Dolan P. Mechanical initiation of intervertebral disc degeneration. Spine (Phila Pa 1976) 2000;25(13):1625–36. [PubMed: 10870137]

55. Joe E, Lee JW, Park KW, et al. Herniation of cartilaginous endplates in the lumbar spine: MRI findings. AJR Am J Roentgenol 2015;204(5):1075–81. [PubMed: 25905944]

56. Theodorou DJ, Theodorou SJ, Kakitsubata S, Nabeshima K, Kakitsubata Y. Abnormal Conditions of the Diskovertebral Segment: MRI With Anatomic-Pathologic Correlation. AJR Am J Roentgenol 2020;214(4):853–61. [PubMed: 32069076]

57. Samartzis D, Mok FPS, Karppinen J, Fong DYT, Luk KDK, Cheung KMC. Classification of Schmorl's nodes of the lumbar spine and association with disc degeneration: a large-scale population-based MRI study. Osteoarthritis Cartilage 2016;24(10):1753–60. [PubMed: 27143364]

58. Kyere KA, Than KD, Wang AC, et al. Schmorl's nodes. Eur Spine J 2012;21(11):2115–21. [PubMed: 22544358]

59. Zehra U, Bow C, Lotz JC, et al. Structural vertebral endplate nomenclature and etiology: a study by the ISSLS Spinal Phenotype Focus Group. Eur Spine J 2018;27(1):2–12.

60. Kaapa E, Luoma K, Pitkaniemi J, Kerttula L, Gronblad M. Correlation of size and type of modic types 1 and 2 lesions with clinical symptoms: a descriptive study in a subgroup of patients with chronic low back pain on the basis of a university hospital patient sample. Spine (Phila Pa 1976) 2012;37(2):134–9. [PubMed: 21415809]

61. Rahme R, Moussa R. The modic vertebral endplate and marrow changes: pathologic significance and relation to low back pain and segmental instability of the lumbar spine. AJNR Am J Neuroradiol 2008;29(5):838–42. [PubMed: 18272564]

62. Splendiani A, Bruno F, Marsecano C, et al. Modic I changes size increase from supine to standing MRI correlates with increase in pain intensity in standing position: uncovering the "biomechanical stress" and "active discopathy" theories in low back pain. Eur Spine J 2019;28(5):983–92. [PubMed: 30982938]

63. Lai A, Iliff D, Zaheer K, et al. Spinal Cord Sensitization and Spinal Inflammation from an In Vivo Rat Endplate Injury Associated with Painful Intervertebral Disc Degeneration. Int J Mol Sci 2023;24(4).

64. Dudli S, Karol A, Giudici L, et al. CD90-positive stromal cells associate with inflammatory and fibrotic changes in modic changes. Osteoarthr Cartil Open 2022;4(3):100287. [PubMed: 36474945]

65. Mosley GE, Evashwick-Rogler TW, Lai A, Iatridis JC. Looking beyond the intervertebral disc: the need for behavioral assays in models of discogenic pain. Ann N Y Acad Sci 2017;1409(1):51–66. [PubMed: 28797134]

66. Wang D, Lai A, Gansau J, et al. Ex vivo biomechanical evaluation of Acute lumbar endplate injury and comparison to annulus fibrosus injury in a rat model. J Mech Behav Biomed Mater 2022;131:105234. [PubMed: 35462160]

67. Merighi A, Carmignoto G, Gobbo S, et al. Neurotrophins in spinal cord nociceptive pathways. Prog Brain Res 2004;146:291–321. [PubMed: 14699971]

68. Kim JS, Ahmadinia K, Li X, et al. Development of an Experimental Animal Model for Lower Back Pain by Percutaneous Injury-Induced Lumbar Facet Joint Osteoarthritis. J Cell Physiol 2015;230(11):2837–47. [PubMed: 25858171]

69. Zachariou V, Goldstein BD. Dynorphin-(1–8) inhibits the release of substance P-like immunoreactivity in the spinal cord of rats following a noxious mechanical stimulus. Eur J Pharmacol 1997;323(2–3):159–65. [PubMed: 9128834]

70. Wan FP, Bai Y, Kou ZZ, et al. Endomorphin-2 Inhibition of Substance P Signaling within Lamina I of the Spinal Cord Is Impaired in Diabetic Neuropathic Pain Rats. Front Mol Neurosci 2016;9:167. [PubMed: 28119567]

71. Zucoloto AZ, Manchope MF, Borghi SM, et al. Probucol Ameliorates Complete Freund's Adjuvant-Induced Hyperalgesia by Targeting Peripheral and Spinal Cord Inflammation. Inflammation 2019;42(4):1474–90. [PubMed: 31011926]

CLINICAL SIGNIFICANCE:

This rat EP microfracture model was validated to induce broad spinal degenerative changes that may be useful to improve understanding of MC-like changes and for therapeutic screening.

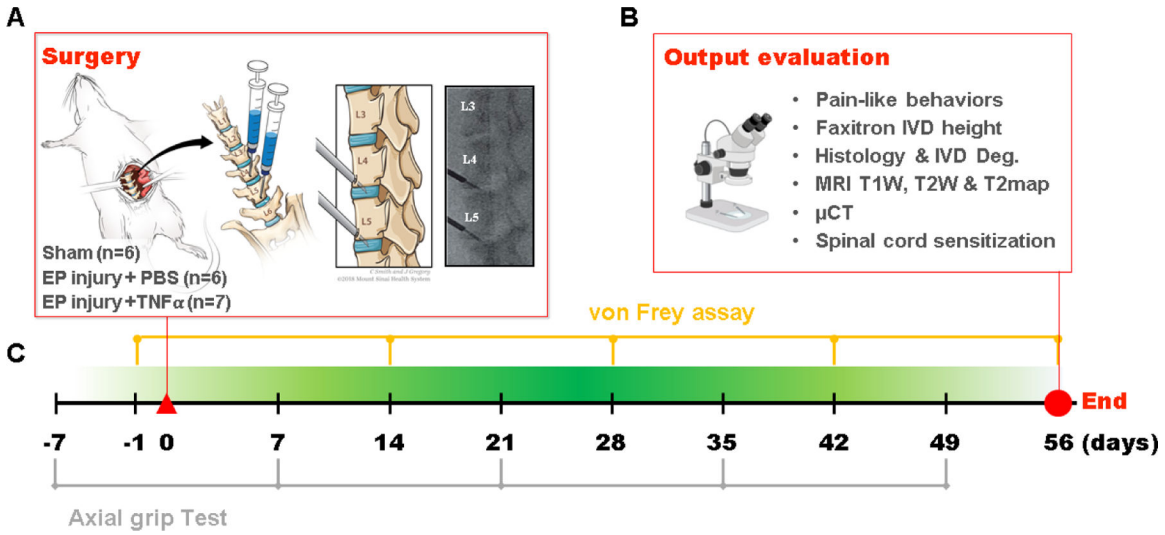

Figure 1:

EP microfracture in-vivo model and study design. A) Schematic of procedure with anterior approach. Experimental groups included Sham (n=6); EP injury + PBS injection (n=6) and EP injury + TNFα injection (n=7). Syringes were inserted through a tight-fitting K-wire channel with syringe depth and bevel position confirmed intraoperatively with a C-Arm to be in the center of NP region to enable injectates to be absorbed by the IVD and marrow and minimize the chance of injectate leakage. B) Output variables after t=56 days (8 weeks). C) Timeline of behavioral measurements.

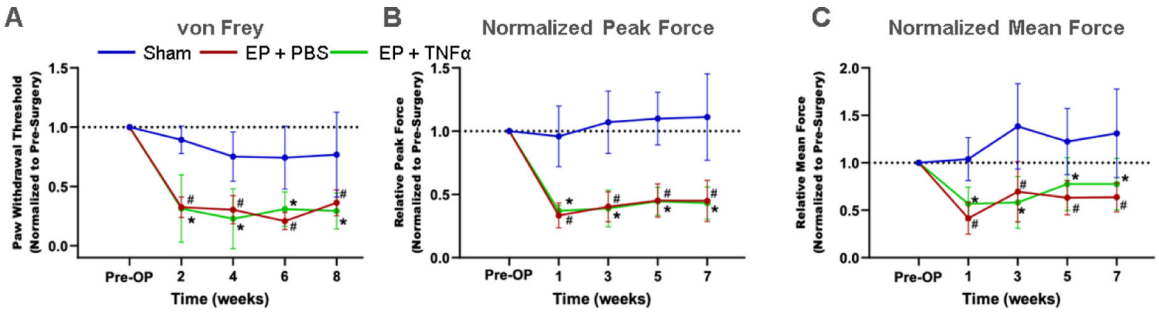

Figure 2:

Behavioral testing demonstrates axial sensitivity and hindpaw mechanical hypersensitivity. A) Paw withdrawal threshold after von Frey test; B) Normalized Peak force and C) normalized mean force after grip test over time # EP+PBS compared to Sham with $p < 0.05$, * EP+TNFα compared to Sham with $p < 0.05$.

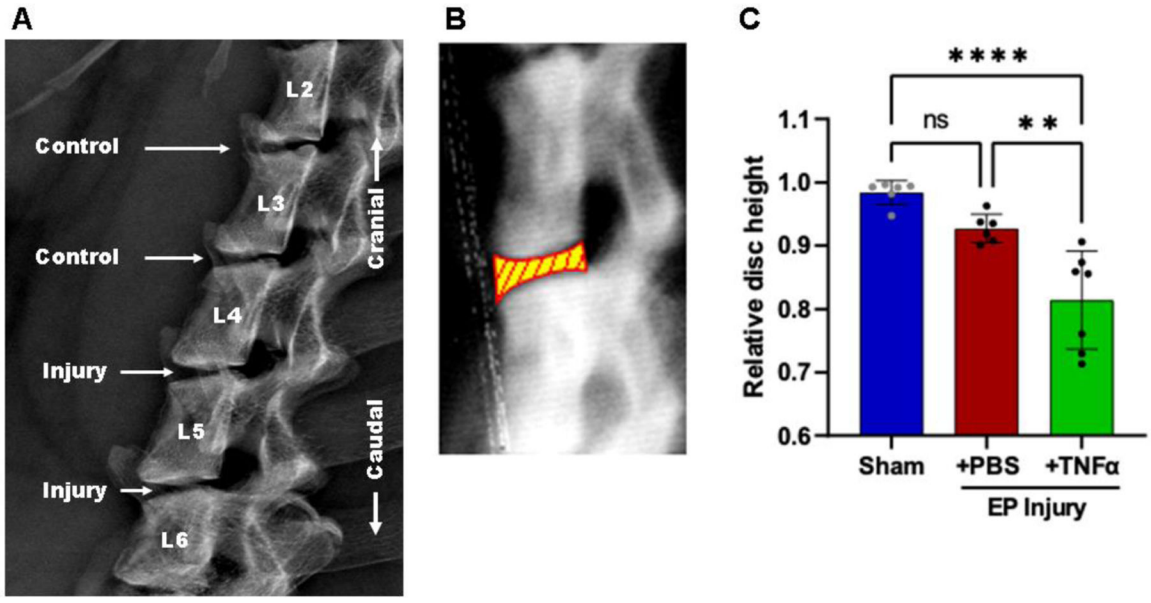

Figure 3:

EP injury causes IVD height loss. A) Faxitron imaging. B) Relative disc height was quantified by tracing the cephalad and caudal vertebral endplates and using a spline program to measure disc heights (yellow and red shape). The relative disc height was calculated by normalizing to pre-operative values at the same level for the same animal. C) Relative disc height was reduced with injury. **and **** indicate significant differences with $p<0.01$ and $p<0.0001$ respectively.

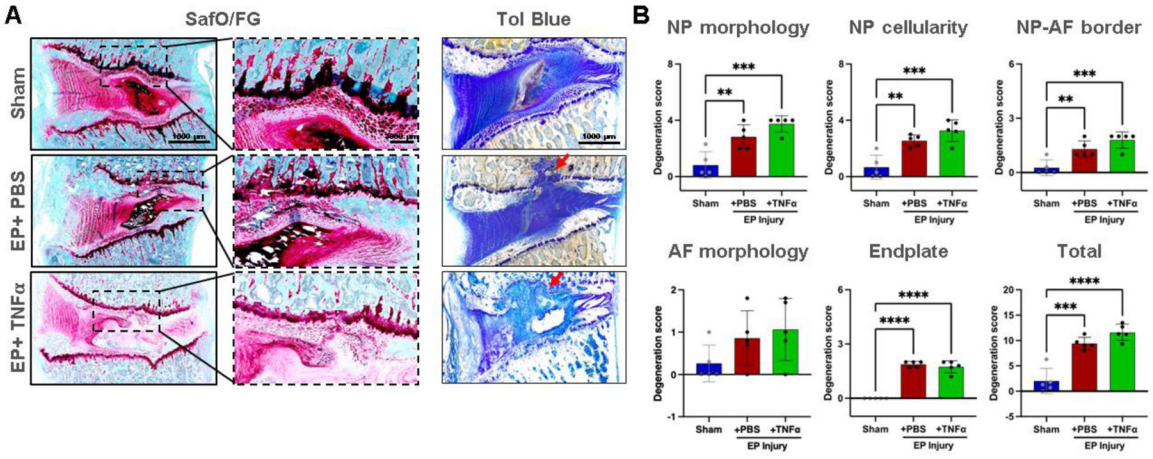

Figure 4:

EP caused IVD degeneration. A) Histology with thin sections stained with Safranin-O/Fast green and thick ground and polished sections stained with Toluidine Blue. Red arrows indicating EP defect. B) IVD degeneration grading using Scoring System [49]. **, *** and **** indicate significant differences with $p<0.01$, $p<0.001$ and $p<0.0001$ respectively.

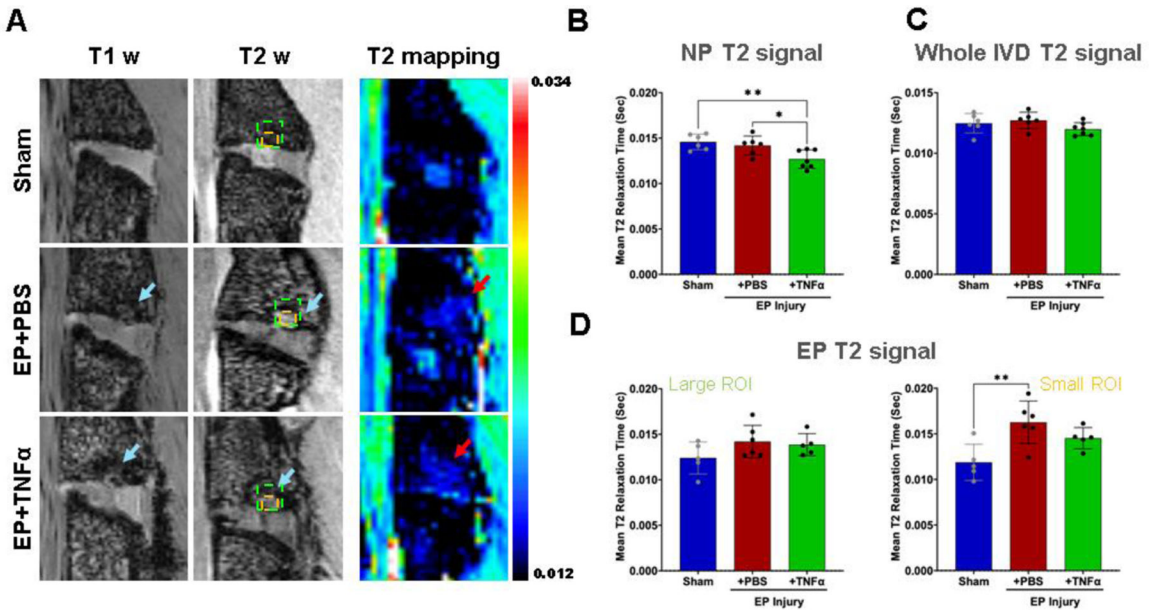

Figure 5:

MRI analyses show significant injury following EP injury for both PBS and TNF α. A) Hypointensity on T1w and T2w MRI (blue arrows) and increased T2 relaxation time (sec) (red arrows) are visible around EP defects. B) Mean T2 relaxation time of NP decreased with injury. C) There was no difference in mean T2 relaxation time of the whole IVD among the 3 groups highlighting that this is a localized injury. D) Mean T2 relaxation time at the EP looking at a larger area (left) and more focused small ROI focused on the microfracture site (right) in which a significant difference between sham and EP=PBS was found. * and ** indicate significant differences between groups with $p<0.05$ and $p<0.01$, respectively.

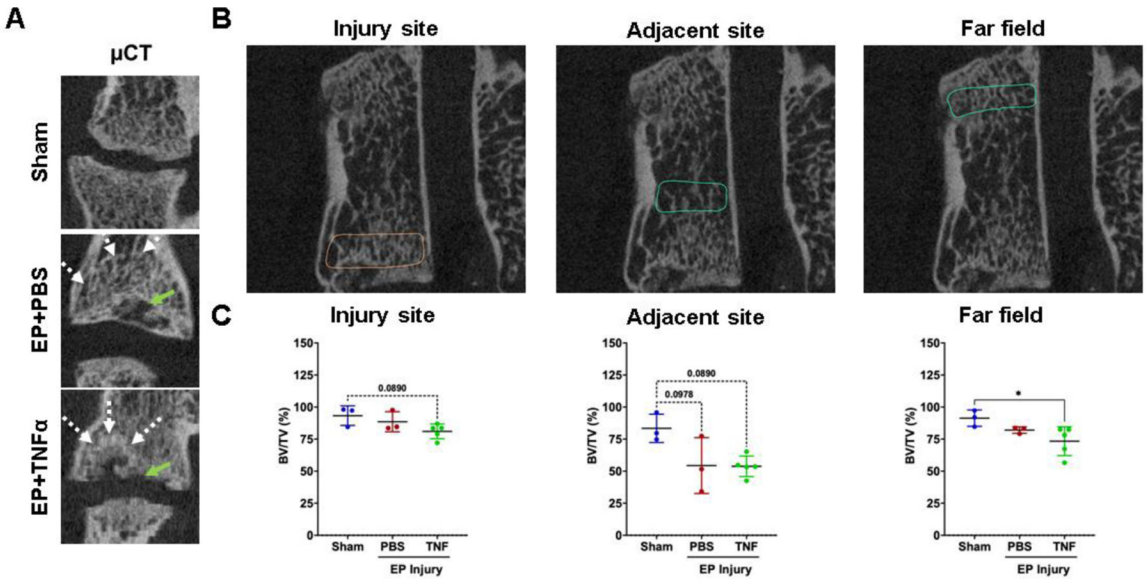

Figure 6:

μCT analyses show vertebral disruption and remodeling at the injury site that is not impacted adjacent or at the far field. A) EP defects are highly visible on μCT, and mid-coronal plane of injured lumbar spinal regions vertebrae show trabecular bone remodeling (white arrow) around EP defect (green arrow). B) Quantitative μCT analyses show extensive injuries at the injury site in the area of the endplate. Bone changes were minimal adjacent to the injury site and not observed in the far field. * indicate significant difference between groups with $p<0.05$.

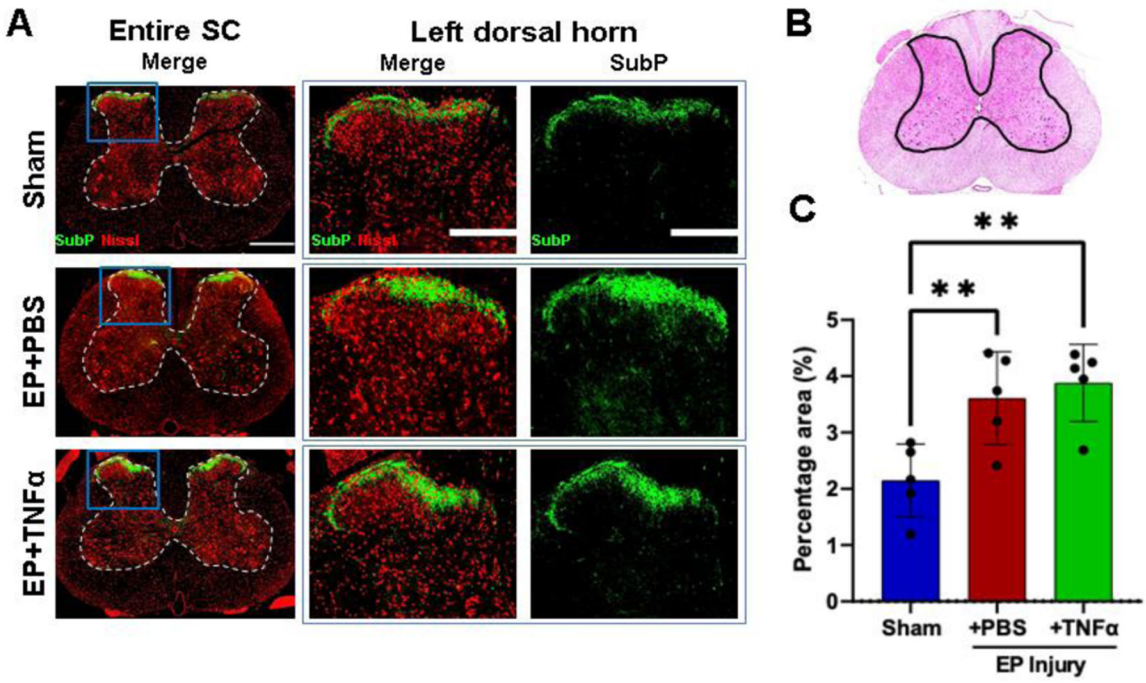

Figure 7:

Spinal Cord Substance P was increased from EP injury. A) Immunofluorescence images of spinal cord (SC) with outlined gray matter showing Neurons (red) and presence of substance P (green) in different groups with focus on dorsal horns. B) hematoxylin and eosin staining of spinal cord with outline of grey matter. C) quantification of SubP in dorsal horn. ** indicate significant difference between groups with $p<0.01$.

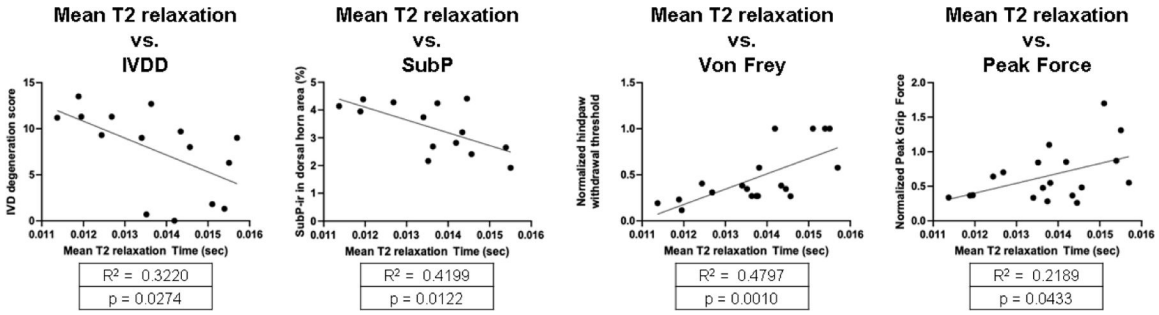

Figure 8:

Correlations of NP T2 with IVDD, Spinal cord (SC) SubP, and pain-related behavioral measurements of von Frey and peak grip force.

Table 1.

Correlation analysis for IVD, vertebral bone and spinal cord crosstalk.

		μCT (injury site)	μCT (adjacent site)	μCT (far field)	EP T2 (large ROI)	EP T2 (small ROI)	Spinal cord SubP
NP T2 signal	Pearson r	**0.645**	0.612	0.454	0.082	−0.046	**−0.708**
	p-value	**0.044** *	0.060	0.188	0.746	0.856	**0.007** *
Whole IVD T2 signal	Pearson r	0.502	0.559	0.242	0.452	**0.490**	−0.552
	p-value	0.140	0.093	0.500	0.060	**0.039** *	0.051
Relative IVD height	Pearson r	0.362	0.531	0.355	0.117	−0.076	**−0.635**
	p-value	0.304	0.114	0.314	0.644	0.764	**0.020** *
Degeneration score	Pearson r	−0.424	**−0.781**	−0.545	0.072	0.283	0.560
	p-value	0.295	**0.022** *	0.163	0.807	0.327	0.073
Spinal cord SubP	Pearson r	**−0.714**	−0.672	−0.312	−0.112	0.311	
	p-value	**0.047** *	0.068	0.451	0.716	0.300	

* indicates significant correlation with $p<0.05$

Table 2.

Correlation analysis to identify important factors contributing to pain-like behaviors.

		NP T2 signal	Relative IVD height	Degeneration score	CT (adjacent site)	EP T2 (large ROI)	EP T2 (small ROI)	Spinal cord SubP
Normalized grip peak force	Pearson r	0.436	**0.481**	**−0.678**	**0.810**	**−0.471**	**−0.604**	**−0.704**
	p-value	0.062	**0.037** *	**0.006** *	**0.005** *	**0.048** *	**0.008** *	**0.007** *
Normalized paw withdrawal threshold	Pearson r	**0.666**	0.444	**−0.757**	0.613	0.005	−0.274	**−0.668**
	p-value	**0.002** *	0.057	**0.001** *	0.059	0.985	0.272	**0.013** *

* indicates significant correlation with $p<0.05$

[a] Normalized grip peak force and normalized paw withdrawal threshold did not significantly correlated with whole IVD T2 signal, μCT (EP), or μCT (far field), $p>0.05$